© Indian Academy of Sciences

ORIGINAL RESULTS

Intensity mapping of post-reionization 21-cm signal and its cross-correlations as a probe of $f(R)$ gravity

CHANDRACHUD B. V. DASH[1], TAPOMOY GUHA SARKAR[1] and
ANJAN KUMAR SARKAR[2,3,*]

[1]Department of Physics, Birla Institute of Technology and Science, Pilani, India.
[2]Raman Research Institute, Bangalore 560080, India.
[3]National Centre for Radio Astrophysics, Tata Institute of Fundamental Research, Pune 411007, India.
*Corresponding author. E-mail: anjansarkarbhp@gmail.com

Abstract. We propose the intensity mapping of the redshifted HI 21-cm signal from the post-reionization epoch as a cosmological probe of $f(R)$ gravity. We consider the Hu–Sawicki family of $f(R)$ gravity models characterized by a single parameter $f_{,R0}$. The $f(R)$ modification to gravity affects the post-reionization 21-cm power spectrum through the change in the growth rate of density fluctuations. We find that a radio interferometric observation with a SKA1-mid-like radio telescope in both auto-correlation and cross-correlation with galaxy weak-lensing and Lyman-α forest may distinguish $f(R)$ models from ΛCDM cosmology at a precision, which is competitive with other probes of $f(R)$ gravity.

Keywords. Cosmology: $f(R)$ gravity—galaxy weak lensing—21-cm signal—Lyman-α forest.

1. Introduction

Einstein's general theory of relativity (GR) has endured a complete century of intensive scrutiny, and has emerged as the most successful theory of gravitation. Several tests on Solar system scales have proved its consistency on small scales (Marchi & Cascioli 2020). However, modifications to the theory of gravity have often been proposed as a way to explain the observed cosmic acceleration (Faraoni 2009). Several observational evidences like Galaxy redshift surveys, Cosmic Microwave Background Radiation (CMBR) observations and supernovae surveys strongly indicate that the energy budget of our Universe is dominated by dark energy—a fluid with energy-momentum tensor that violates the strong energy condition (Perlmutter *et al.* 1997; Hinshaw *et al.* 2003; Spergel *et al.* 2003; Riess *et al.* 2016). The cosmological constant (Λ) treated as a fluid with an equation of state $p = -\rho$ is the most popular candidate for dark energy in the framework of classical general relativity (Padmanabhan 2003). However, the Λ CDM, model suffers from several theoretical and observational difficulties (Weinberg 1989; Carroll 2001; Riess *et al.* 2016; Zhao *et al.* 2017). In the matter sector, scalar fields have often been used to model various properties of dynamical and clustering dark energy (Ratra & Peebles 1988; Turner & White 1997; Caldwell *et al.* 1998; Armendariz-Picon *et al.* 2001; Bento *et al.* 2002; Padmanabhan & Choudhury 2002; Bagla *et al.* 2003; Nojiri *et al.* 2006). Extensive literature is available on the diversity of such models and their general treatment using model-independent parametrizations Chevallier & David (2001); Linder (2003); Barboza & Alcaniz (2008).

Alternatively, a modification of Einstein's theory can mimic dark energy without requiring an exotic fluid (Amendola & Tsujikawa 2010). In $f(R)$ theory, the Ricci scalar, R appearing in the Einstein-Hilbert action, is replaced by a general function of R (Nojiri & Odintsov 2007; Sotiriou & Liberati 2007; Capozziello & Francaviglia 2008; Sotiriou & Faraoni 2010) as:

$$S = \frac{1}{2\kappa} \int d^4x \sqrt{-g}\, f(R) + S_m, \tag{1}$$

where $\kappa = (8\pi G_N)/c^4$ and S_m the action for matter. The $f(R)$ modification naturally has its imprint on the background comsological evolution and growth of structures.

Tomographic intensity mapping of the neutral hydrogen Hɪ distribution (Chang *et al.* 2008; Bull *et al.* 2015; Obuljen *et al.* 2018) using radio observations of the redshifted 21-cm radiation is a powerful probe of cosmic evolution and structure formation in the post reionization epoch (Bharadwaj & Sethi 2001; Bharadwaj *et al.* 2001; Bharadwaj & Pandey 2003; Bharadwaj & Srikant 2004; Wyithe & Loeb 2007, 2008, 2009; Loeb & Wyithe 2008; Visbal *et al.* 2009). The epoch of reionization is believed to be completed by redshift $z \sim 6$ (Gallerani *et al.* 2006). Following the complex phase transition characterizing the epoch of reionization (EoR), some remnant neutral hydrogen remained clumped in the dense self-shielded damped Ly-α (DLA) systems (Wolfe *et al.* 2005). These DLA systems are the dominant source of the Hɪ 21-cm signal in the post-reionization era. Intensity mapping experiments aim to map out the collective Hɪ 21-cm radiation without resolving the individual gas clouds. The redshifted 21-cm signal from the post-reionization epoch as a biased tracer (Bagla *et al.* 2010; Guha Sarkar *et al.* 2012) of the dark matter distribution imprints a host of astrophysical and cosmological information. It is, thereby a direct probe of large scale matter distribution, growth of perturbations and the expansion history of the Universe. Observationally, the post-reionization signal has two key advantages: first, since the galactic synchrotron foreground scales as $\sim(1 + z)^{2.6}$, the lower redshifts are far less affected by the galactic foreground. Second, in the redshift range $z \leq 6$, the astrophysical processes of the EoR are absent, whereby the background UV radiation field does not have any feature imprinted on the 21-cm signal.

The $f(R)$ modification to gravity will affect the 21-cm power spectrum through its signature on cosmic distances, the Hubble parameter and the growth rate of density perturbations. We consider a Hu–Sawicki form of $f(R)$, and investigate the possibility of differentiating such a modification from the standard ΛCDM model.

In this paper, our objective is to make error projections on parameters of a $f(R)$ gravity theory using the post-reionization 21-cm power spectrum in auto- and cross-correlations. For cross-correlation of the 21-cm signal, we have considered two dark matter tracers: (a) galaxy weak lensing and (b) the Lyman-α forest. We investigate observational strategies with the upcoming square kilometer array (SKA) towards

constraining $f(R)$ theories at precession levels competitive, if not significantly better than the next generation of supernova Ia observations, galaxy surveys and CMB experiments.

2. Cosmology with $f(R)$ gravity

We consider a spatially flat Universe comprising of radiation (density, ρ_γ) and non-relativistic matter (density, ρ_m). In a $f(R)$ gravity theory, the Einstein's field equation and its trace for a Friedman–Lemitre–Robertson–Walker metric (FLRW) with a scale factor $a(t)$ and Hubble parameter $H = \dot{a}(t)/a(t)$, reduces to (Tsujikawa *et al.* 2009)

$$3H^2 f_{,R} - \frac{1}{2}(Rf_{,R} - f) + 3H\dot{f}_{,R} = \kappa^2(\rho_m + \rho_\gamma),$$
(2)

$$Hf_{,R} - 2f_{,R}\dot{H} - \ddot{f}_{,R} = \kappa^2\left(\rho_m + \frac{4}{3}\rho_\gamma\right),$$
(3)

where $f_{,R} = \partial f(R)/\partial R$ and the '.' denotes a differentiation with respect to the cosmic time t. The Ricci scalar, R is given by $R = 6(2H^2 + \dot{H})$. It is convenient to express the above equations in terms of the following set of dimensionless variables:

$$x_1 \equiv -\frac{\dot{f}_{,R}}{Hf_{,R}}, \quad x_2 \equiv -\frac{f}{6H^2 f_{,R}},$$

$$x_3 \equiv \frac{R}{6H^2}, \quad x_4 \equiv \frac{\kappa^2\rho_\gamma}{3H^2 f_{,R}}.$$

In terms of these quantities, the dynamical evolution of the density parameters can be obtained by solving the following set of autonomous first-order differential equations (Tsujikawa *et al.* 2009)

$$x_1' = -1 - x_3 - 3x_2 + x_1^2 - x_1 x_3 + x_4,$$
(4)

$$x_2' = \frac{x_1 x_3}{m} - x_2(2x_3 - 4 - x_1),$$
(5)

$$x_3' = -\frac{x_1 x_3}{m} - 2x_3(x_3 - 2),$$
(6)

$$x_4' = -2x_3 x_4 + x_1 x_4,$$
(7)

where $' ' = \mathrm{d}/\mathrm{d}\ln(a)$ and m measures the deviation from ΛCDM model defined as:

$$m \equiv \frac{d\ln f_{,R}}{d\ln R} = \frac{Rf_{,RR}}{f_{,R}}.$$

These equations form a 4-dimensional coupled dynamical system, which can be integrated numerically for a given $f(R)$ and with suitable initial conditions. Solution to the above coupled ODEs can be used to determine the dynamics of the density parameters and

map a $f(R)$ gravity theory to a dark energy with an effective equation of state (EoS), $w_{\text{eff}}(z)$ as:

$$\Omega_m \equiv \frac{\kappa^2 \rho_m}{3H^2 f_{,R}} = 1 - (x_1 + x_2 + x_3 + x_4), \tag{8}$$

$$\Omega_\gamma \equiv x_4, \tag{9}$$

$$\Omega_{\text{DE}} \equiv x_1 + x_2 + x_3, \tag{10}$$

$$w_{\text{eff}} \equiv -\frac{1}{3}(2x_3 - 1). \tag{11}$$

A wide variety of $f(R)$ models have been proposed (Capozziello 2002; Carroll *et al.* 2004; Hu & Sawicki 2007a; Nojiri & Odintsov 2007). The functional form of $f(R)$ is chosen so that the model is phenomenologically satisfactory. We expect the $f(R)$ cosmology to be indistinguishable from the ΛCDM at high redshifts, where the latter is well constrained from CMBR observations. At low redshifts, the accelerated expansion history should be close to the ΛCDM predictions and on Solar system scales, the proposed $f(R)$ model should be consistent with the ΛCDM model as a limiting case.

We consider the $f(R)$ gravity model proposed by Hu–Sawicki (HS), where the functional form of $f(R)$ is given by (Hu & Sawicki 2007a; Amendola & Tsujikawa 2010):

$$f(R) = R - \mu R_c \frac{(R/R_c)^2}{(R/R_c)^2 + 1}. \tag{12}$$

Here, μ and R_c are two non-negative parameters in the model, where R_c is the present day value of the Ricci scalar. The expansion rate H for a viable $f(R)$ gravity theories is expected to be close to the concordance ΛCDM (Hu & Sawicki 2007b) predictions. The quantity $f_{,R}$ plays a crucial role to quantify the deviation of $f(R)$ gravity models from GR, whereby $f_{,R}$ behaves like an extra degree of freedom that acts similar to a scalar field. We may write:

$$f_{,R} = -2f_0 \frac{R}{H_0^2} \left[1 + \left(\frac{R}{R_c} \right)^2 \right]^{-2}, \tag{13}$$

with $|f_0| \equiv (\mu H_0^2)/R_c$ as the only free parameter.

To recover standard GR results in Solar system tests, the present day value of $f_{,R}$ is restricted to $\log_{10} |f_{,R0}| < -6$ (Hu & Sawicki 2007a). Further, the second derivative $f_{,RR} = d^2f(R)/dR^2 > 0$ to avoid ghost and tachyonic solutions (Amendola *et al.* 2007). Weak lensing peak abundance studies have provided strong constraints on $\log_{10} |f_{,R0}| < -4.82$ and -5.16 with WMAP9 and Planck15 priors, respectively. Tight constraints are also obtained from weak lensing peak statistics study with $\log_{10} |f_{,R0}| < -4.73$

(WMAP9) and $\log_{10} |f_{,R0}| < -4.79$ (Planck 2013; Liu *et al.* 2016). In our work, we adopt the fiducial value $\log_{10} |f_{,R0}| = -5$ from observations (Cataneo *et al.* 2015; Liu *et al.* 2016).

Growth of large scale structure (LSS) offers a unique possibility to constrain cosmological models. The quantity of interest is the growth rate of matter density perturbations $f_g(k, z) \equiv (d\ln\delta_m(k, z))/(d\ln a)$. which is sensitive to the expansion history of the Universe. In the linear perturbation theory, and on sub-horizon scales ($k/a \gg H$), the evolution of matter density perturbations $\delta_m(k, z)$ is dictated by the differential equation (Boisseau *et al.* 2000; Song *et al.* 2007; Tsujikawa *et al.* 2008, 2009)

$$\ddot{\delta}_m + 2H\dot{\delta}_m - 4\pi G_{\text{eff}}(a, k)\rho_m \delta_m \simeq 0, \tag{14}$$

where G_{eff} is an effective gravitational constant, which is related to standard Newtonian gravitational constant (G_N) as:

$$G_{\text{eff}}(a, k) = \frac{G_N}{f_{,R}} \left[1 + \frac{(k^2/a^2)(f_{,RR}/f_{,R})}{1 + 3(k^2/a^2)(f_{,RR}/f_{,R})} \right]. \tag{15}$$

In $f(R)$ theories, G_{eff} is a scale-dependent function (Baghram & Rahvar 2010). The scale dependence of the growing mode of density fluctuations is widely exploited to differentiate the structure formation beyond standard model of cosmology. In obtaining the approximate Equation (14), we have incorporated the assumption that oscillating modes are negligible compared to the modes induced by matter perturbations and also $\dot{f}_{,R} \approx 0$ on sub-horizon scales of interest (Tsujikawa *et al.* 2009).

Figure 1 shows the departure of the the growth rate $f_g(z, k)$ for the $f(R)$ theory with $\log_{10} |f_{,R0}| = -5$ from the ΛCDM prediction. We know that the growth rate is scale-independent and depends only on redshift for the ΛCDM model. Thus, the k-dependence seen in the figure arises purely from the $f(R)$ modification to gravity. Since different modes grow differently, the evolution has an additional contribution towards changing the shape of the cosmological power spectrum. The departure is small at very low redshifts and also very high redshifts and increases monotonically with k for a given redshift. We find that a departure of $>12\%$ is seen in the redshift window $0.5 < z < 1.5$ for $k > 0.5$ Mpc^{-1}.

In Figure 2, we have shown the linear growth rate $f_g(z, k)$ for ΛCDM and $f(R)$ with $\log_{10} |f_{,R0}| = -5$ at a redshift $z = 2.3$. At smaller scales (large k modes), the scale-dependent growth become more prominent
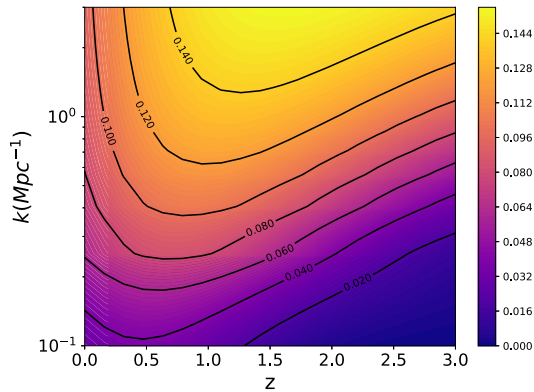
Figure 1. Departure of the growth rate $f_g(z, k)$ for the $f(R)$ theory with $\log_{10}|f_{,R0}| = -5$ from the ΛCDM prediction. We plot the quantity $|(f_g - f_g^{\Lambda\text{CDM}})/f_g^{\Lambda\text{CDM}}|$ in the (z, k) plane.
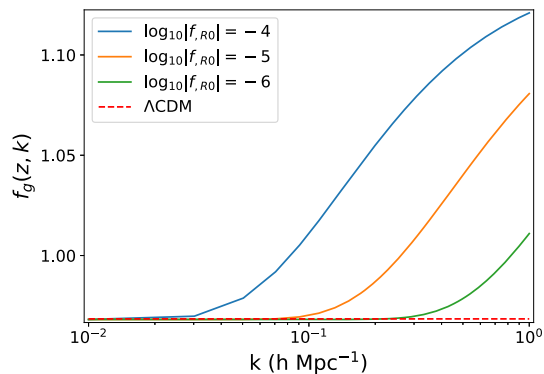

Figure 2. Growth rate $f_g(z, k)$ for the $f(R)$ theory of $\log_{10}|f_{,R0}| = -5$ model. We have also shown the results for $\log_{10}|f_{,R0}| = -4$ and $\log_{10}|f_{,R0}| = -6$ model for comparison purpose. The dotted bottom shows scale-independent ΛCDM prediction. The fiducial redshift chosen as $z = 2.3$.

and larger scales (small k modes), $f(R)$ gravity coincide with ΛCDM. We have also shown the $f_g(k, z)$ for $\log_{10}|f_{,R0}| = -4$ and $\log_{10}|f_{,R0}| = -6$ gravity model for comparison purpose only.

2.1 *Matter power spectrum*

$f(R)$ gravity has a significant impact on structure formation in low-density regions through a scale-dependent growth factor because of enhancement of gravitational forces. The modification to the force law in modified gravity theories is highly constrained from local tests (Will 2014). It is also well studied that $f(R)$ modification to gravity will induce non-linearities in the power spectrum through mechanisms like chameleon (Mota & Shaw 2007), dilaton effect (Brax *et al.* 2014), etc. The shape of the matter power spectrum is sensitive to the choice of cosmological model and as such
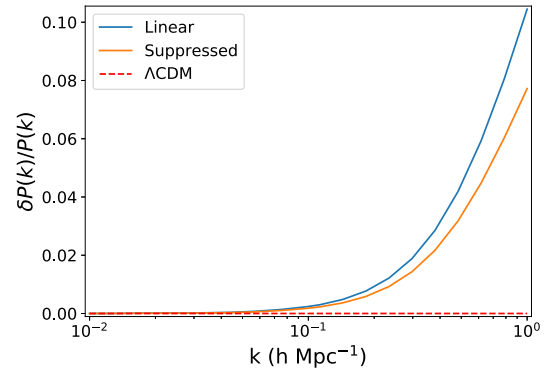
Figure 3. Departure of the matter power spectrum $P(z, k)$ for the $f(R)$ theory with $\log_{10}|f_{,R0}| = -5$ from the Λ CDM prediction. We plot the quantity $(P_{f(R)}(k, z) - P_{\Lambda\text{CDM}}(k, z))/(P_{\Lambda\text{CDM}}(k, z))$ at redshift $z = 2.3$.

it is sensitive probe of the underlying theory of gravity or dark energy. We model the power spectrum in $f(R)$ gravity models as:

$$P_{f(R)}(k) = \frac{P_{\text{Lin}}}{(1 + k^2/k_{\text{trunc}}^2)^2} \, e^{-(k/k_s)^2}, \tag{16}$$

where P_{Lin} is the linear matter power spectrum. In our analysis, we have used the analytic fitting function by Hu–Eisenstein for P_{Lin} (Eisenstein & Hu 1998). We have used the fitting parameters (k_{trunc}, k_s) for the suppressed matter power spectrum from Brax & Valageas (2019) for $f(R)$ gravity models. $P(k, z)$ is obtained by multiplying the square of the growing mode with this. We remind ourselves that the growing mode is scale-dependent for $f(R)$ models and is scale-independent for ΛCDM model.

Figure 3 shows the relative deviation of matter power spectrum of $f(R)$ gravity theory from ΛCDM at a fiducial redshift $z = 2.3$. The topmost curve corresponds to linear theory prediction and the one below shows the suppressed matter power spectrum due to the additional factor introduced in Equation (16). The relative deviation of $P_{\text{Lin}}(k)$ from its ΛCDM counterpart grows at smaller scales, because the mass of the scalar field yields a characteristic scale dependence for the linear growing mode. Moreover, on linear scales, there is no additional chameleon screening mechanism.

Many simulation results show that the deviation is significantly suppressed due to screening mechanism (Li *et al.* 2013; Arnold *et al.* 2019). The additional prefactor in Equation (16) is fitted for mildly nonlinear behavior and reproduces the suppressed matter power spectrum with sub-percent accuracy without requiring the full non-linear simulations (refer Figure 5 in Li *et al.* 2013).

3. 21-cm signal from the post-reionization era

Bulk of the low-density hydrogen gets completely ionized by the end of the reionization epoch around $z \sim 6$ (Gallerani *et al.* 2006). A small fraction of HI that survives the process of reionization is believed to remain confined in the over-dense regions of the IGM. These clumped, dense DLAs (Wolfe *et al.* 2005) remain neutral as they are self-shielded from the background ionizing radiation. They store $\sim$80% of the HI at $z < 4$ (Prochaska *et al.* 2005) with HI column density greater than 2×10^{20} atoms cm^{-2} (Lanzetta *et al.* 1995a; Storrie-Lombardi *et al.* 1996; Peroux *et al.* 2003) and are the dominant source of the 21-cm radiation in the post-reionization epoch. The clustering properties of these DLA clouds suggest that they are associated with galaxies and located in regions of highly non-linear matter over densities (Zwaan *et al.* 2005; Cooke *et al.* 2006; Nagamine *et al.* 2007). The 21-cm signal from the post-reionization epoch has been extensively studied Subramanian & Padmanabhan (1993); Bharadwaj & Sethi (2001); Bharadwaj *et al.* (2001); Bharadwaj & Pandey (2003); Bharadwaj & Srikant (2004); Visbal *et al.* (2009); Wyithe & Loeb (2009). The emitted flux from individual clouds is extremely weak ($<$10 μJy). These individual DLA clouds are unlikely to be detected in radio observations, even with futuristic telescopes. However, in an intensity mapping experiment, one does not aim to resolve the individual sources. The collective emission forms a diffused background in all radio-observations at the observation frequencies $<$1420 MHz. Fluctuations of this signal on the sky plane and across redshift, maps out the three dimensional tomographic image of the Universe.

Several assumptions simplify the modeling of the post-reionization HI signal. These are either motivated from implicit observations or from numerical simulations.

- In the post-reionization epoch, there is an enhancement of population of the triplet state of HI due to the Wouthheusen field coupling. This makes the spin temperature T_s much greater than the CMB temperature T_γ. Thus, the 21-cm radiation is seen in emission in this epoch against the background CMBR (Madau *et al.* 1997; Bertotti *et al.* 2003; Loeb & Zaldarriaga 2004). For $z \leq 6$, the spin temperature and gas kinetic temperature remain strongly coupled through Lyman-α scattering or collisional coupling (Madau *et al.* 1997).
- Extensive study of the Lyman-α absorption lines in quasar spectra indicates that in the redshift range $1 \leq z \leq 3.5$, the cosmological density parameter of the neutral gas has a value $\Omega_{gas} \sim 10^{-3}$ (Prochaska *et al.* 2005). Thus, the mean neutral fraction is $\bar{x}_{HI} = \Omega_{gas}/\Omega_b \sim 2.45 \times 10^{-2}$, which does not evolve in the entire redshift range $z \leq 6$.
- On the large cosmological scales of interest, HI peculiar velocities are assumed to be determined by the dark matter distribution. Thus, peculiar velocity manifests as a redshift space distortion anisotropy in the 21-cm power spectrum.
- The discrete nature of DLA sources is not considered. The corresponding Poisson noise owing to this discrete sampling is neglected assuming that the number density of the DLA emitters is very large (Bharadwaj & Srikant 2004).
- HI perturbations are generated by a Gaussian random process. We do not consider any non-Gaussianity and thereby the statistical information is contained in the two-point correlation or the power spectrum.
- Galaxy redshift surveys and numerical simulations show that the galaxies are biased tracers of the underlying dark matter distribution (Mo *et al.* 1996; Dekel & Lahav 1999; Yoshikawa *et al.* 2001). If we assume that HI in the post-reionization epoch is housed predominantly in dark matter halos, we may expect the gas to trace the underlying dark matter density field with a bias $b_T(k, z)$ defined as:

$$b_T(k, z) = \left[\frac{P_{HI}(k, z)}{P(k, z)} \right]^{1/2},$$

where $P_{HI}(k, z)$ and $P(k, z)$ denote the HI and dark matter power spectra, respectively. The bias function quantifies the nature of HI clustering in the post-reionization epoch. Further, the fluctuations in the ionizing background may also contribute to $b_T(k, z)$ (Wyithe & Loeb 2009). On scales below the Jean's length, the linear density contrast of HI gas is related to the dark matter density contrast though a scale-dependent function (Fang *et al.* 1993). However, on large scales, the bias is known to be scale-independent, though the scales above which the bias is linear, is sensitive to the redshift being probed. Several authors have now demonstrated the nature of HI bias using N-body simulations (Bagla *et al.* 2010; Guha Sarkar *et al.* 2012; Carucci *et al.* 2017). The simulations are based on the principle of populating dark matter halos in a certain mass range with gas and thereby identifying them as DLAs.

These simulations show that the large scale linear bias grows monotonically with redshift for $1 < z < 4$ (Marín *et al.* 2010). This feature is shared by galaxy bias as well (Fry 1996; Mo *et al.* 1996, 1999). There is a steep rise of the 21-cm bias on small scales. This is because in the absence of small mass halos as is expected from the CDM power spectrum and consequently, the H I being distributed only in larger halos. A fitting formula for the bias $b_T(k, z)$ as a function of both redshift z and scale k has been obtained from numerical simulations (Guha Sarkar *et al.* 2012) of the post-reionization signal as:

$$b_T(k, z) = \sum_{m=0}^{4} \sum_{n=0}^{2} c(m, n) k^m z^n. \qquad (17)$$

The critical density for collapse is smaller in $f(R)$ gravity models, which leads to a significant suppression of bias, i.e., $b_T^{f(R)} < b_T^{GR}$. This has been seen in numerical simulations (Aviles *et al.* 2018; Arnold *et al.* 2019). Though the fitting function for b_T (17) is obtained from ΛCDM simuation, we used the same form for $f(R)$ gravity assuming the bias is not significantly different in the redshifts of our interest. However, we have kept the bias as free parameter, which we have eventually marginalized over. We kept the third-order component of polynomial bias as the free parameter because we know on large scale, the bias is completely indistinguishable from ΛCDM and suppression shows up only on small scales. For $\log_{10}|f_{,R0}| = -5$ model, our used bias fitting function is well within the error bars and can be used safely (Aviles *et al.* 2018).

We have used these simulation results in our modeling of the post-reionization epoch.

Adopting all the assumptions discussed above, the power spectrum of post-reionization H I 21-cm brightness temperature fluctuations from redshift z is given by (Bertotti *et al.* 2003; Bharadwaj *et al.* 2009):

$$P_{HI}(\mathbf{k}, z) = \bar{T}(z)^2 \bar{x}_{HI}^2 b_T(k, z)^2$$
$$\times (1 + \beta_T(k, z)\mu^2)^2 P(k, z), \qquad (18)$$

where $\mu = \hat{\mathbf{k}} \cdot \hat{\mathbf{n}}$, $\beta_T(k, z) = f_g(k, z)/b_T(k, z)$, and

$$\bar{T}(z) = 4.0 \text{ mK } (1 + z)^2 \left(\frac{\Omega_{b0}h^2}{0.02}\right) \left(\frac{0.7}{h}\right) \frac{H_0}{H(z)}. \qquad (19)$$
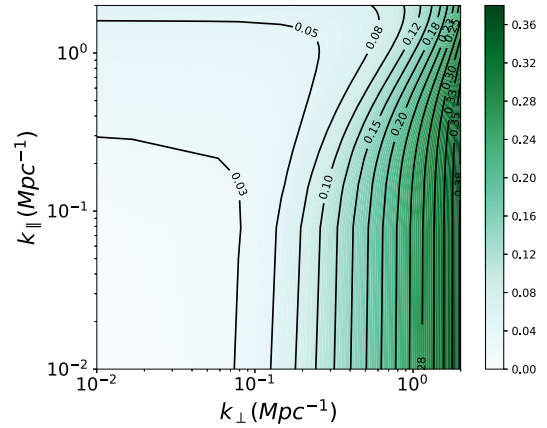
Figure 4. The 21-cm power spectrum in the $(k_\parallel, k_\perp)$ space at the observing frequency $\nu_0 = 710$ MHz.

The term $f_g(z, k)\mu^2$ H I peculiar velocities (Bharadwaj & Sethi 2001; Bertotti *et al.* 2003), which, as we mentioned, is also sourced by the dark matter fluctuations.

The $f(R)$ modification affects the 21-cm power spectrum through the change in the redshift space distortion parameter $\beta_T(k, z)$ and $P(k, z)$. Figure 4 shows the 21-cm power spectrum at $z = 1$ in the $(k_\parallel, k_\perp)$ space. The asymmetry in the signal is indicative of redshift space distortion and is sensitive to $\beta_T(k, z)$. We emphasize that $(\bar{x}_{HI}, \beta_T(k, z))$ along with the cosmological parameters completely model the post-reionization 21-cm signal. We note that the product $b_T^2 \bar{x}_{HI}$, which appears in the overall amplitude of the 21-cm signal is a largely unknown parameter and depends largely on the H I modeling. We shall, therefore, be interested in constraining the function $\beta_T(k, z)$ from some radio-interferometric observation of the signal. We shall marginalize our Fisher matrix projections over the overall amplitude to make error projections.

We shall now investigate the possibility of constraining the function $\beta_T(k, z)$ and thereby put observational bounds on $|f_{,R0}|$ from a radio-interferometric observation of the signal.

3.1 *Observed 21-cm power spectrum*

The quantity of interest in radio-interferometric observation is the complex visibility $\mathcal{V}(\mathbf{U}, \nu)$ measured as function of baseline $\mathbf{U} = (u, v)$ and observing frequency ν. Considering an observation frequency band width and defining $\Delta\nu$ as the difference from the central observing frequency, a further Fourier transform in $\Delta\nu$ gives us the visibility $v(\mathbf{U}, \tau)$ as a function of delay channel τ. The measured visibility can be written as a sum of signal $s(\mathbf{U}, \tau)$ and noise $n(\mathbf{U}, \tau)$ as

$v(\mathbf{U}, \tau) = s(\mathbf{U}, \tau) + n(\mathbf{U}, \tau)$. The signal $s(\mathbf{U}, \tau)$ can be written as:

$$s(\mathbf{U}_a, \tau_m) = \frac{2k_{\mathrm{B}}}{\lambda^2} \int \frac{d^3\mathbf{k}}{(2\pi)^3} \, G(\mathbf{k}, \mathbf{U}_a, \tau_m) \widetilde{\delta T_b}(\mathbf{k}), \quad (20)$$

where $\widetilde{\delta T_b}(\mathbf{k})$ denotes the fluctuations of the 21-cm brightness temperature in Fourier space. The transformation kernel G is given by:

$$G(\mathbf{k}_\perp, k_\parallel, \mathbf{U}_a, \tau_m) = \widetilde{\mathcal{A}}\left(\frac{\mathbf{k}_\perp r}{2\pi} - \mathbf{U}_a\right) \widetilde{\mathcal{B}}\left(\frac{k_\parallel r'}{2\pi} - \tau_m\right),$$

where $\widetilde{\mathcal{A}}(\mathbf{U})$ and $\widetilde{\mathcal{B}}(\tau)$ denote the Fourier transform of the telescope beam $A(\vec{\theta})$ and the frequency response window function $B(\Delta v)$, respectively. We use r to denote comoving distance to the observing redshift $z = (1420 \text{ MHz per } v) - 1$ and $r' = dr(v)/dv$. The signal covariance matrix is defined as $\langle s(\mathbf{U}_a, \tau_m) s^*(\mathbf{U}_b, \tau_n)\rangle = C^S_{(a,m),(b,n)}$ and is given by:

$$C^S = \left(\frac{2k_{\mathrm{B}}}{\lambda^2}\right)^2 \frac{1}{r^2 r'} \int d^2\mathbf{U} d\tau \, G(\mathbf{k}, \mathbf{U}_a, \tau_m)$$
$$\times \, G^*(\mathbf{k}, \mathbf{U}_b, \tau_n) P_{\mathrm{HI}}(\mathbf{k}), \quad (21)$$

where

$$\mathbf{k} = \left(\frac{2\pi \mathbf{U}}{r}, \frac{2\pi \tau}{r'}\right).$$

The noise in the visibilities measured at different baselines and frequency channels are uncorrelated. If we define the noise covariance matrix as $C^N = \langle n(\mathbf{U}_a, \tau_m) \, n^*(\mathbf{U}_b, \tau_n)\rangle$, we have:

$$C^N = \left(\frac{2k_{\mathrm{B}}}{\lambda^2}\right)^2 \left(\frac{\lambda^2 T_{\mathrm{sys}}}{A_e}\right)^2 \frac{B}{t} \delta_{m,n} \delta_{a,b}, \quad (22)$$

where t is the correlator integration time and B is the observing bandwidth. The system temperature T_{sys} can be written as a contribution from the instrument and the sky as $T_{\mathrm{sys}} = T_{\mathrm{inst}} + T_{\mathrm{sky}}$, where

$$T_{\mathrm{sky}} = 60 \text{ K} \left(\frac{v}{300 \text{ MHz}}\right)^{-2.5}.$$

We first investigate the possibility of constraining the scale-dependent function $\beta_T(k, z_{\mathrm{fid}})$. We divide the observational range $k_{\min}$ to $k_{\max}$ into N_{bin} bins and constrain the values of $\beta_T(k_i)$ at the middle of the bin k_i using a Fisher matrix analysis. The departure from the ΛCDM model for the fiducial $\log_{10}|f_{,R0}| < -5$ model for a range of k values, peaks around $z \sim 1$. We choose the observational central frequency to be 710 MHz corresponding to this redshift. We first consider an OWFA (Bharadwaj *et al.* 2015; Sarkar *et al.* 2017a, 2018a) like array, which is the upgraded version of the Ooty radio telescope and is expected to operate as an linear radio-interferometric array. The OWFA is a 530

m long and 30 m wide parabolic cylindrical reflector that is placed along the north–south direction on a hill that has the same slope ($\sim 11°$) as the latitude of the place. This makes it possible to track a given patch of sky by rotating the cylinder about the long axis of the telescope. The OWFA has 1056 dipoles in total that are equally placed at ~ 0.5 m apart from each other along the long axis of the telescope. OWFA is capable of operating in two independent simultaneous radio-interferometric modes: PI and PII. The OWFA PII has 264 antennas in total, the radio signals from four consecutive dipoles have been combined to form a single antenna element. The OWFA PII has the smallest baseline length, $d = 1.92$ m that corresponds to the distance between the two consecutive antennas in the array. The OWFA PII has an operating bandwidth, $B = 39$ MHz (for detailed specifications, see Bharadwaj *et al.* 2015). The full covariance matrix is given by:

$$C_{ab} = C^S + \frac{C^N}{N_r}, \quad (23)$$

where $N_r = 264 - a$ is the redundancy of the baselines. The Fisher matrix is given by:

$$F_{ij} = \frac{1}{2} \sum_m C^{-1}(m)_{ab} C(m)_{bc,i} C^{-1}(m)_{cd} C(m)_{bc,j}, \quad (24)$$

where i and j runs over the parameters $\beta_T(k_1)$, $\beta_T(k_2), \ldots, \beta_T(k_{N_{\mathrm{bin}}})$. The error on the ith parameter is obtained from the Cramer Rao bound as $\sqrt{F_{ii}^{-1}}$. We found that in the k-range $0.06 < k < 1.32$ $\beta_T(k)$ can be measured in 4 bins at $>9\%$ for 500×50 h observation with 50 independent pointings. Since the maximum departure of $\beta_T(k)$ from the ΛCDM is $\sim 11\%$ in the k-range of interest, such an observation will at its best be able to distinguish between a $\log_{10}|f_{,R0}| = -5$ at a $\sim 1 - \sigma$ level and $\log_{10}|f_{,R0}| = -4$ at $\sim 2 - \sigma$ level.

For stronger constraints, we now consider a SKA1-mid-type of radio array. We consider a binning in visibility $\Delta\mathbf{U}$ and a total observing time T_0 causing a reduction of noise variance by a factor N_p, where N_p is the number of visibility pairs in the bin given by $N_p = N_{\mathrm{vis}}(N_{\mathrm{vis}} - 1)/2 \approx N_{\mathrm{vis}}^2/2$, where N_{vis} is the number of visibilities in the bin measured in time T_0. We may write:

$$N_{\mathrm{vis}} = \frac{N_{\mathrm{ant}}(N_{\mathrm{ant}} - 1)}{2} \frac{T_o}{t} \rho(\mathbf{U}) \delta^2 U, \quad (25)$$

where N_{ant} is the total number of antennas in the array and $\rho(\mathbf{U})$ is the baseline distribution function. In

general, the baseline distribution function is given by a convolution:

$$\rho(\mathbf{U}) = c \int d^2\mathbf{r} \rho_{\text{ant}}(\mathbf{r}) \rho_{\text{ant}}(\mathbf{r} - \lambda\mathbf{U}), \qquad (26)$$

where c is fixed by normalization of $\rho(\mathbf{U})$ and ρ_{ant} is the distribution of antennas. Further, if we assume a uniform frequency response over the entire observation bandwidth B and a Gaussian beam for the telescope:

$$\int d\tau \widetilde{\mathcal{B}}(\tau - \tau_m)\widetilde{\mathcal{B}}^*(\tau - \tau_n) = B\delta_{mn} \qquad (27)$$

and

$$\int d^2\mathbf{U}\mathcal{A}(\mathbf{U} - \mathbf{U}_a)\mathcal{A}^*(\mathbf{U} - \mathbf{U}_b) \approx \frac{\lambda^2}{A_e}\delta_{a,b}, \qquad (28)$$

where A_e is the effective area of the antenna dishes. With these simplifications, we may then write:

$$C^S \approx \left(\frac{2k_B}{\lambda^2}\right)^2 \frac{B\lambda^2}{r^2 r' A_e} P_{\text{HI}}\left(\frac{2\pi\mathbf{U}_a}{r}, \frac{2\pi\tau_m}{r'}\right)\delta_{m,n}\delta_{a,b}.$$

The 21-cm power spectrum is not spherically symmetric, due to redshift space distortion, but is symmetric around the polar angle ϕ. Using this symmetry, we would want to sum all the Fourier cells in an annulus of constant $(k, \mu = \cos\theta = k_{\parallel}/k)$ with radial width Δk and angular width $\Delta\theta$ for a statistical detection with improved SNR. The number of independent cells in such an annulus is:

$$N_c = 2\pi k^2 \Delta k \Delta\mu \frac{\text{Vol}}{(2\pi)^3}, \qquad (29)$$

where the volume 'Vol' of the intensity mapping survey is given by Vol $= (r^2\lambda^2 r' B)/A_e$. Thus, the full covariance matrix may be written as:

$$C^{\text{Tot}} = \frac{1}{\sqrt{N_c}}\left[C^S + \frac{C^N}{N_p}\right]. \qquad (30)$$

The covariance matrix is diagonal owing to the binning in U since different baselines, which get correlated due to the telescope beam are now uncorrelated. Further, to increase the sensitivity, we consider the angle averaged power spectrum by averaging over μ. Thus, we have:

$$P_{\text{HI}}(k) = \bar{T}(z)^2 \bar{x}_{\text{HI}}^2 b_T^2\left(1 + \frac{2}{3}\beta_T + \frac{1}{5}\beta_T^2\right)P(k, z) \qquad (31)$$

and the corresponding variance is obtained by summing:

$$\delta P_{\text{HI}}(k) = \left[\sum_\mu \frac{1}{\delta P_{\text{HI}}(k, \mu)^2}\right]^{-1/2}, \qquad (32)$$

where $\delta P_{\text{HI}}(k, \mu) = (A_e r^2 r')/(\lambda^2 B)C^{\text{Tot}}$.
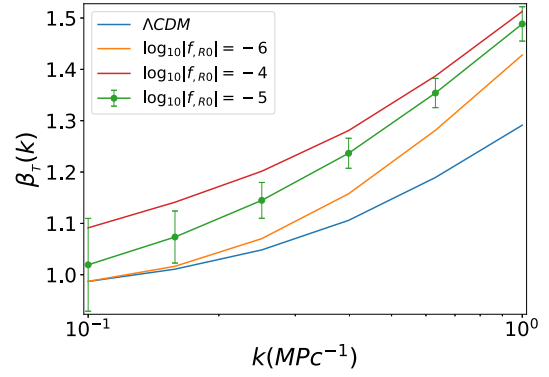
Figure 5. Variation of $\beta_T(k, z_{\text{fid}})$ at the fiducial redshift $z_{\text{fid}} = 1$ for various Hu–Sawcki $f(R)$ models. The ΛCDM prediction is also shown. We also show the $1-\sigma$ error bars on β_T at six logarithmically spaced k-bins in the observed range of scales for the fiducial model with $\log_{10}|f_{,R0}| = -5$.

The fisher matrix for parameters λ_i may be written as:

$$F_{ij} = \sum_k \frac{1}{\delta P_{\text{HI}}^2(k)} \frac{\partial P_{\text{HI}}(k)}{\partial\lambda_i} \frac{\partial P_{\text{HI}}(k)}{\partial\lambda_j}. \qquad (33)$$

We consider a radio telescope with an operational frequency range of 350 MHz–14 GHz. We consider 250 dish antennae, each with a diameter of 15 m and an efficiency of 0.7. To calculate the normalized baseline distribution function, we assumed that baselines are distributed, such that the antenna distribution falls off as $1/r^2$. We also assumed that there is no baseline coverage <30 m. We assume $T_{\text{sys}} = 60$ K and an observation bandwidth of 128 MHz. We assume $\Delta U = U_{\text{min}} = 50$, over which the signal is averaged.

Figure 5 shows the variation of $\beta_T(k, z_{\text{fid}})$ at the fiducial redshift $z = 1$ corresponding to the observing central frequency of 710 MHz. The monotonic rise of $\beta_T(k, z_{\text{fid}} = 1.0)$ owes its origin to both the monotonic growth of $f_g(k)$ and also a slow decrease of $b_T(k, z_{\text{fid}} = 1.0)$ in the k-range of interest. The behavior is similar for different values of $\log_{10}|f_{,R0}|$. The ΛCDM result is seen to coincide with the $f(R)$ prediction on large scales. We note that the $\log_{10}|f_{,R0}| = -6$ matches with the ΛCDM model for $k < 0.15$ Mpc^{-1}. We consider a fiducial $\log_{10}|f_{,R0}| = -5$ for our analysis. The k-range between the smallest and largest baselines in binned as $\Delta k = \alpha k$, where $\alpha = (1/N_{\text{bin}})\ln(U_{\text{max}}/U_{\text{min}})$, with $(U_{\text{min}}, U_{\text{max}}) = (50, 550)$. We consider 400×50 h observation in 50 independent pointings. The $1 - \sigma$ errors on $\beta_T(k_i)$ are obtained from the Fisher matrix analysis, where the overall normalization of the power-spectrum is marginalized over. We found that for $k > 0.4$ Mpc^{-1}, the $\log_{10}|f_{,R0}| = -5$ can be differentiated from the ΛCDM model at a sensitivity of $>5\sigma$, if

Table 1. The 68% $(1 - \sigma)$ marginalized errors on $\log_{10} |f_{,R0}|$ and Ω_{m0}.

Model	$\log_{10} |f_{R0}|$	Ω_{m0}
$f(R)$	-5 ± 0.62	0.315 ± 0.005

we consider 6k-bins. On larger scales $k < 0.4$ Mpc^{-1} and the $f(R)$ models with $-6 < \log_{10} |f_{,R0}| < -4$ remain statistically indistinguishable from the ΛCDM model. Thus, it appears that 21-cm observations of the post-reionization epoch may only be able to constrain $f(R)$ theories on relatively small scales.

Instead of constraining the binned function $\beta_T(k)$, we investigate the possibility of putting bounds on $\log_{10} |f_{,R0}|$ from the given observation. Marginalizing over the overall amplitude of the power spectrum, we are thus interested in two parameters $(\Omega_{m0}, \log_{10} |f_{,R0}|)$. The $1 - \sigma$ bounds on $\log_{10} |f_{,R0}|$ obtained from the marginalized Fisher matrix is given in Table 1. Our error projection may be compared with constraints obtained from other observational probes Table 2. We found that our projected constraints are competitive with constraints obtained from diverse probes.

The radio-interferometric observation of the post-reionization H I 21-cm signal, thus holds the potential of providing robust constraints on $f(R)$ models.

4. Cross-correlation of 21-cm signal with galaxy weak lensing

Weak lensing (Waerbeke & Mellier 2003; Munshi *et al.* 2008) of background source galaxies by large scale structure (cosmic shear) has been extensively studied as a powerful cosmological probe (Jain & Seljak 1997; Eisenstein & Hu 1998; Huterer & White 2002; Takada & Jain 2003; Heavens 2003; Knox *et al.* 2004; Miyazaki *et al.* 2007; Hoekstra & Jain 2008; Takada & Jain 2009). The quantity of interest to us is the amplification matrix (Waerbeke & Mellier 2003; Munshi *et al.* 2008), which quantifies the distortions due to gravitational lensing. These distortions allow to analyze large scale structures and map the matter distribution, on a broad range of scales. Noting that scalar perturbations cannot induce any rotation, only one has shear (γ) and convergence (κ) effects in the lensed distorted image of a galaxy. This weak shear/convergence signal is superposed on the intrinsic ellipticities and irregularities of background galaxy images (Treu 2010). We are interested in the statistical properties of these distortion fields. The angular

power spectrum of the shear field is identical to that of the convergence field, whereby we shall only be looking at the convergence field. The weak-lensing convergence field on the sky is given by a weighed line of sight integral (Waerbeke & Mellier 2003) of the overdensity field δ:

$$\kappa(\vec{\theta}) = \int_0^{\chi_s} \mathcal{A}_\kappa(\chi)\delta(\chi\vec{\theta}, \chi)d\chi, \tag{34}$$

where χ denotes the comoving distance and

$$\mathcal{A}_\kappa(\chi) = \frac{3}{2}\left(\frac{H_0}{c}\right)^2 \Omega_{m0} \frac{g(\chi)\chi}{a(\chi)},$$

with

$$g(\chi) = \int_\chi^{\chi_s} n(z)\frac{dz}{d\chi'}\frac{\chi' - \chi}{\chi'}d\chi'. \tag{35}$$

The weight function appearing in the kernel incorporates all the sources distributed according to a distribution function $n(\chi)$ up to χ_s. We have assumed that the source galaxies are distributed as (Huterer *et al.* 2006):

$$n(z) = n_0 \left(\frac{z}{z_0}\right)^\alpha \exp\left[-\left(\frac{z}{z_0}\right)^\beta\right]. \tag{36}$$

In this work, we have considered a weak-lensing survey, where $z_0 = 0.5, \alpha = 2$ and $\beta = 1$ (Takada & Jain 2009). On small angular scales (typically for $\ell > 10$) where flat sky approximation is reasonable, we can use the Limber approximation (Limber 1954) in Fourier space and write the weak-lensing convergence angular power spectrum as:

$$C_\kappa^\ell = \frac{9}{4}\left(\frac{H_0}{c}\right)^4 \Omega_{m0}^2 \int_0^{\chi_s} \frac{g^2(\chi)}{a^2(\chi)} P\left(\frac{\ell}{\chi}, \chi\right) d\chi, \tag{37}$$

where P denotes the matter power spectrum. The noise for the convergence angular power spectrum is given by ΔC_κ^ℓ, where

$$\Delta C_\kappa^\ell = \sqrt{\frac{2}{(2\ell + 1)f_{\text{sky}}}}\left(C_\kappa^\ell + \frac{\sigma_\epsilon^2}{n_g}\right). \tag{38}$$

Here, the Poisson noise is dictated by the total galaxy count:

$$n_g = \int_0^{\chi_s} n(z)\frac{dz}{d\chi'}d\chi'. \tag{39}$$

The fraction of the sky observed in the weak-lensing survey is assumed to be $f_{\text{sky}} = 0.5$ and we adopt $\sigma_\epsilon = 0.4$ as the galaxy-intrinsic rms shear (Hu 1999). The factor $(2\ell + 1)$ in the denominator counts the number of samples of C_κ^ℓ for a given ℓ.

On large scales, the redshifted H I 21-cm signal from post-reionization epoch known to be biased tracers

Table 2. Bounds on $p = \log_{10} |f_{,R0}|$ from other probes.

Probe of $f(R)$ gravity	Bound on $\log_{10} |f_{,R0}|$
GW merger, GW170817	$p < -2.52$ (Jana & Mohanty 2019)
Suyaev Zeldovich clusters PLANCK	$-5.81 < p < -4.40$ (Peirone *et al.* 2017)
Weak-lensing peak statistics	$-5.16 < p < -4.82$ (Liu *et al.* 2016)
CMB + cluster + SN + H_0 + BAO	$p < -3.89$ (Schmidt *et al.* 2009)

of the underlying dark matter distribution. Assuming HI perturbations are generated by a Gaussian random process and incorporating the effect of redshift space distortion, the fluctuations of the 21-cm brightness temperature $\delta_T(\mathbf{r})$ in Fourier space may be written as:

$$\delta_T(\mathbf{r}) = \frac{1}{(2\pi)^3} \int e^{i\mathbf{k}\cdot\mathbf{r}} \Delta_T(\mathbf{k}),$$

where

$$\Delta_T(\mathbf{k}) = \mathcal{A}(z) \left[1 + \beta_T \mu^2 \right] \Delta(\mathbf{k}), \tag{40}$$

with

$$\mathcal{A}_T = 4.0 \text{ mK } b_T \bar{x}_{\text{HI}} (1+z)^2 \left(\frac{\Omega_{b0} h^2}{0.02} \right)$$
$$\times \left(\frac{0.7}{h} \right) \left(\frac{H_0}{H(z)} \right). \tag{41}$$

Here, Δ denotes the fluctuations of the dark matter overdensity field in Fourier space, b_T is a bias function and $\bar{x}_{\text{HI}}$ is the mean neutral fraction, which is assumed to remain constant in the post-reionization epoch ($z < 6$). We adopt the value $\bar{x}_{\text{HI}} = 2.45 \times 10^{-2}$ from (Lanzetta *et al.* 1995b; Péroux *et al.* 2003; Noterdaeme *et al.* 2009; Zafar *et al.* 2013). We define a quantity on the sky:

$$T(\hat{\mathbf{n}}) = \frac{1}{\chi_s - \chi_0} \sum_{\chi_0}^{\chi_s} \Delta\chi \, \delta_T(\chi\hat{\mathbf{n}}, \chi), \tag{42}$$

as the integral of the 3D 21-cm brightness temperature field along the radial direction.

In a radio interferometric observation, the quantity of interest is the complex visibilities, which are Fourier transformation of the intensity distribution on the sky. Using a flat sky approximation, we define visibilities as:

$$V_T(\vec{\mathbf{U}}) = \int d^2\vec{\theta} a(\vec{\theta}) T(\vec{\theta}) e^{-2\pi i \vec{\mathbf{U}}\cdot\vec{\theta}},$$
$$V_\kappa(\vec{\mathbf{U}}) = \int d^2\vec{\theta} \kappa(\vec{\theta}) e^{-2\pi i \vec{\mathbf{U}}\cdot\vec{\theta}}, \tag{43}$$

where $\vec{\theta}$ is the angular coordinates on the flat sky plane, $a(\vec{\theta})$ denotes the beam function of the telescope measuring the angular coverage of the 21-cm survey. The

mulipole ℓ is related to baseline $\vec{\mathbf{U}}$ as $\ell = 2\pi U$. The aperture function $\tilde{a}(\vec{\mathbf{U}})$ is the Fourier transformation of $a(\vec{\theta})$. Defining the cross-correlation angular power spectrum $C^{T\kappa}(U)$ as $\langle V_T(\vec{\mathbf{U}}) V_\kappa^*(\vec{\mathbf{U}}') \rangle = C^{T\kappa}(U)$, we have (Dash & Guha Sarkar 2021) for a sharp aperture $\tilde{a}(\vec{\mathbf{U}})$,

$$C^{T\kappa}(U) = \frac{1}{\pi(\chi_s - \chi_0)} \sum_{\chi_0}^{\chi_s} \frac{\Delta\chi}{\chi^2} \mathcal{A}_T \mathcal{A}_\kappa$$
$$\times \int_0^\infty dk_\parallel \left[1 + \beta_T \frac{k_\parallel^2}{k^2} \right] P(k, \chi), \tag{44}$$

with

$$k = \sqrt{k_\parallel^2 + \left(\frac{2\pi\vec{\mathbf{U}}}{\chi} \right)^2}.$$

The auto-correlation angular power spectra may be similarly written as (Dash & Guha Sarkar 2021):

$$C^{TT}(U) = \frac{1}{\pi(\chi_2 - \chi_1)^2} \sum_{\chi_1}^{\chi_2} \frac{\Delta\chi}{\chi^2} \mathcal{A}_T^2$$
$$\times \int_0^\infty dk_\parallel \left[1 + \beta_T \frac{k_\parallel^2}{k^2} \right]^2 P(k, \chi), \tag{45}$$

$$C^{\kappa\kappa}(U) = \frac{1}{\pi} \int_0^{\chi_s} \frac{d\chi}{\chi^2} \mathcal{A}_\kappa^2 \int_0^\infty dk_\parallel P(k, \chi). \tag{46}$$

We follow the formalism in (Dash & Guha Sarkar 2021) and considered the cross-correlation with the 21-cm signal averaged over the signals from redshift slices to improve the signal-to-noise ratio. As a note of caution, we point out that working in the Fourier basis in the flat sky approximation necessarily makes the signal non-ergodic when we consider correlation between two-time slices (due to time evolution of all the relevant cosmological quantities). Further, one also notes the complications arising from the inseparability of the baseline $\mathbf{U}$ (transverse) from the frequency (radial) in this formalism.

The angular power spectrum for two redshifts separated by Δz is known to decorrelate very fast in the radial

direction (Bharadwaj & Pandey 2003). In this work, we consider the summation in Equation (44) over redshift slices, whose width is larger than the typical decorrelation length. Each term in the sum can thus be thought of as an independent observation of the signal. Thus, the noise in each term in the summation may be thought of as an independent random variable and the mutual noise covaraiances between the slices may be ignored. Thus, the errors in $C^{T\kappa}(U)$ is given by:

$$\sigma_{T\kappa} = \sqrt{\frac{(C^{\kappa\kappa} + \langle N^\kappa \rangle)(C^{TT} + \langle N^T \rangle)}{(2\ell + 1)N_c}}, \quad (47)$$

where N_c is the number of redshift slices over which tthe signal is averaged in Equation (44) and $\langle N^{F_{HI}} \rangle$ and $\langle N^\kappa \rangle$ correspond to the average of the noise power spectrum for F_{HI} and κ, respectively.

We compute the expected bounds on HS $f(R)$ gravity free parameter, which measures the deviation from ΛCDM models. We have considered telescope specifications of the upcoming SKA1-mid radio interfeoremeter. We have used the cosmological parameters from Planck (2018) results $(\Omega_{m_0}, \Omega_{b_0}, H_0, n_s, \sigma_8, \Omega_K) = (0.315, 0.0496, 67.4, 0.965, 0.811, 0)$ from (Aghanim *et al.* 2020) for our subsequent analysis. The model galaxy distribution function $(n(z, z_0))$ is adopted from Takada & Jain (2004) and Huterer *et al.* (2006). The cross-correlation can only be computed in an overlapping volume for the weak lensing and 21-cm intensity mapping survey. We choose the frequency band 400–950 MHz of SKA1-mid, since it corresponds to a redshift range that overlaps with the redshift range of the weak-lensing survey. SKA1-mid has 250 antennae. The diameter of each antenna is taken to be 13.5 m and system temperature (T_{sys}) assumed to be 40 K for the entire redshift range. We also assume that full frequency band will be sub-divided into smaller frequency bands of 32 MHz. The details of the SKA1-mid telescope specifications including the baseline distribution can be found in the SKA website.[1]

Cross-correlation of CMBR weak lensing and H I 21-cm power spectrum has been studied earlier (Sarkar 2010; Dash & Guha Sarkar 2021). In this paper, we address the cross-correlation with galaxy weak-lensing. A typical galaxy weak-lensing survey is different from CMBR weak-lensing survey for the following reason. The CMBR temperatures are drawn from a Gaussian distribution, where the galaxies are the tracers of the underlying matter distribution, which are at least small scales and completely non-linear. However, we have not
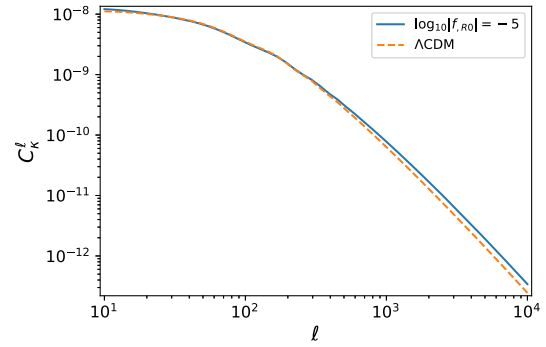
Figure 6. Auto-correlation signal as a function of multiples for modified $f(R)$ model. The dotted line shows the ΛCDM prediction. The source redshift of a galaxy assumed to be $z_s = 1.0$.

incorporated the effects of non-linearity in our analysis as we are working in the regime of the linear perturbation theory. Second, the galaxy surveys are purely 3D, while CMB anisotropies are in general a function of angular position ℓ on sky. Figure 6 shows theoretically expected convergence auto-correlation angular power spectrum signal for ΛCDM and HS model with free parameter $\log_{10} |f_{,R0}| = -5$ for reference. The source redshift of galaxy assumed to be $z_s = 1$. It can be seen that on larger scales, the $f(R)$ model predictions agree with ΛCDM. A significant deviation from classical GR is only found beyond a scale $\ell > 200$ because of the scale-dependent growing mode. Similar results are obtained from simulations in Higuchi & Shirasaki (2016) and Li & Shirasaki (2018). We also note that the deviation from ΛCDM in a range of scale $200 < \ell < 3000$ is typically around 10–15%.

We are interested in the cross-correlation signal of H I 21-cm and galaxy lensing. The cross-correlation signal takes the same shape as of convergence auto-correlation signal. We have computed the cross-correlation signal using Equation (44). Figure 7 shows the difference of the H I 21-cm and galaxy weak lensing angular cross-correlation power spectrum for HS parametrization with $\log_{10} |f_{,R0}| = -5$ from ΛCDM. The 1-σ error bars on ΛCDM shows the HS model with $\log_{10} |f_{,R0}| = -5$ can be differentiated from ΛCDM at a level of $> 2\sigma$ sensitivity using galaxy density $n_g = 60$ arcmin^{-2} and radio interferometric observation time $T_{obs} = 600$ h.

The Fisher analysis is used to put bound on the parameter $\log_{10} |f_{,R0}|$ using the cross-correlation signal. Assuming the fiducial value of $\log_{10} |f_{,R0}| = -5$ and marginalizing over the overall amplitude, redshift distortion parameter (β_T), we found the $1 - \sigma$ bounds, on $\log_{10} |f_{,R0}|$ as shown in Table 3.
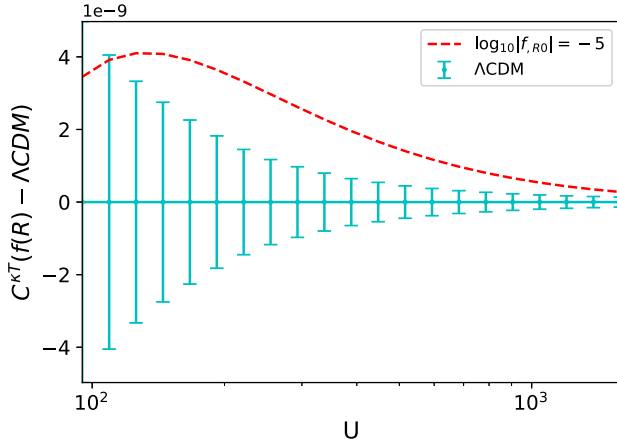
Figure 7. Difference of H I 21-cm-galaxy weak lensing cross-correlation power spectrum for the HS model with free parameter $\log_{10} |f_{,R0}| = -5$ from the standard ΛCDM. The $1 - \sigma$ error bars on ΛCDM shown assuming the galaxy density $n_g = 60$ arcmin^{-2} and observation time $T_{\rm obs} = 600$ h.

Table 3. The 68% $(1 - \sigma)$ constraints of $\log_{10} |f_{,R0}|$ and Ω_{m0} from H I 21-cm and galaxy lensing cross power spectrum.

Model	$\log_{10} |f_{,R0}|$	Ω_{m0}
HS-$f(R)$	-5 ± 0.59	0.315 ± 0.10

5. Cross-correlation of 21-cm signal with Lyman-α forest

5.1 *Lyman-α forest power spectrum*

Lyman-α forest traces out the small fluctuations in the H I density in the IGM along the line of sight (LoS) to distant background quasars and shows an absorption feature in the quasar spectra. The quantity of interest is the transmitted QSO flux through the Lyman-α. The fluctuating Gunn–Peterson effect allows us to write:

$$\mathcal{F} = \bar{\mathcal{F}} e^{-A(1+\delta)^{\Gamma}}, \tag{48}$$

where $\bar{\mathcal{F}}$ denotes the mean transmitted flux, Γ depend on the slope of the temperature-density power spectrum and the factor A depends on the H I photoionization rate, which is difficult to measure independently and assumed to be nearly ~ 1. Several simulation works of Lyman-α forest shows the transmitted flux $\delta_{\mathcal{F}} = (\bar{\mathcal{F}} - F)/\bar{F} \propto \delta$ (Carucci *et al.* 2017).

The influence of $f(R)$ gravity theory in the Lyman-α forest power spectrum has been studied extensively (Arnold *et al.* 2015; Brax & Valageas 2019). Fitting formulae for Lyman-α forest power spectrum

$(P_{\mathcal{FF}}(k))$ are usually written in terms of the matter power spectrum $P(k)$ with several prefactors to match numerical simulations. We follow Brax & Valageas (2019) to model the Lyman-α power spectrum in $f(R)$ gravity theory. The Lyman-α power spectrum can be written in terms of matter power spectrum as follows:

$$P_{\mathcal{FF}}(k, z) = \frac{(1 + \beta_{\mathcal{F}} \mu^2)^2}{(1 + f_g k_{\parallel}/k_{NL})} P(k, z) e^{-(k_{\parallel}/k_{\rm th})^2}, \tag{49}$$

where μ is the cosine of the angle between LoS ($\hat{n}$) and the wave vector ($\vec{k}$), so that $\mu = \hat{k} \cdot \hat{n} = k_{\parallel}/k$. Here, $\beta_{\mathcal{F}}$ is the large scale aniosotropy parameter or so called the redshift distortion factor and $k_{\rm th}$ is the thermal brodening cutoff wave number. We will use Equation (49) to compute the 3D and 1D Lyman-α auto correlation power spectrum. The Equation (49) gives the 3D Lyman-α power spectrum in the redshift space. The observed 1D power spectrum along LoS is given by the standard integral:

$$P_{\mathcal{FF}}^{1D}(k_{\parallel}) = \frac{1}{(2\pi)^2} \int dk_{\perp} P_{\mathcal{FF}}(k). \tag{50}$$

Both Lyman-α and the H I 21-cm signal from the post-reionization epoch are extremely useful tools to probe underlying theory of gravity and put stringent constraints on cosmological parameters individually. However, on large scale, both trace the dark matter density field motivating us to investigate their cross-correlation signal (Guha Sarkar *et al.* 2010). The cross-correlation of the Lyman-α and H I 21-cm signal has been studied for the ΛCDM model extensively (Guha Sarkar *et al.* 2010; Sarkar & Datta 2015; Carucci *et al.* 2017; Sarkar *et al.* 2018b). In this paper, we shall extend it to $f(R)$ gravity models. The Lyman-α and H I 21-cm signal can be written using the formalism in Sarkar & Datta (2015) and Equation (49). We choose a fiducial redshift $z = 2.3$ for this analysis. Figure 8 shows the 3D cross-correlation power spectrum in $(k_{\perp}, k_{\parallel})$ plane for $\log_{10} |f_{,R0}| = -5$. The asymmetry in cross-signal arises because of Kaiser effect in the redshift space. However, the deviation of asymmetry is much enhanced than the auto-correlation signal. Figure 8 shows the 3D Lyman-α and H I 21-cm cross-correlation power spectra at a fiducial redshift $z = 2.3$. The fiducial redshift chosen to be $z = 2.3$ as the QSO distribution is known to peaks at $z = 2.25$ and falls off as we move away from peak (Abolfathi *et al.* 2018). The deviation of spherical symmetry in power spectrum arises because of the linear redshift space distortion parameters $\beta_{\mathcal{F}}$ and β_T. We next use the cross-correlation signal to put constraints on the parameter $\beta_T(k, z)$. We have used the cosmological parameters from Planck (2018)
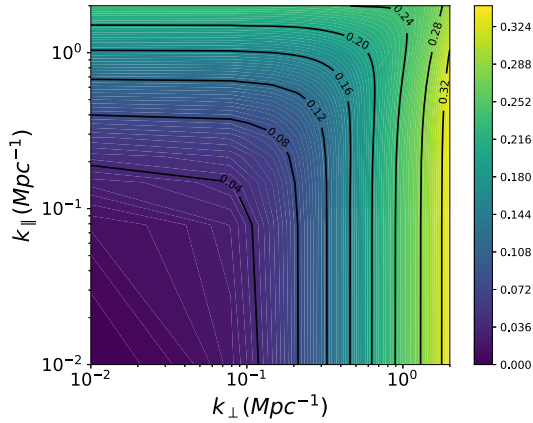
Figure 8. The 3D cross-correlation power spectrum in redshift space for $f(R)$ gravity at a fiducial redshift $z = 2.3$. The asymmetry in the signal is indicative of redshift space distortion.
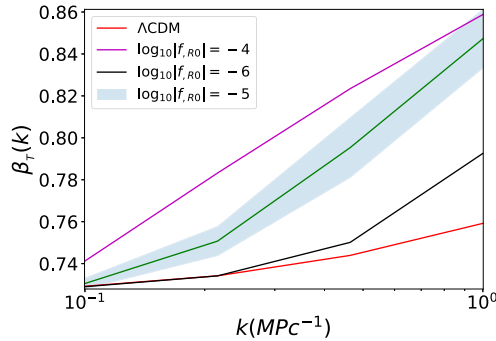
Figure 9. Redshift distortion parameter β_T at a fiducial redshift $z = 2.3$. The $1 - \sigma$ marginalized error is shown by the shaded region on the top of fiducial $f(R)$ gravity $\log_{10}|f_{,R0}| = -5$ model. We have also shown the different parameterized $f(R)$ gravity models and ΛCDM for comparison.

results $(\Omega_{m_0}, \Omega_{b_0}, H_0, n_s, \sigma_8, \Omega_K) = (0.315, 0.0496, 67.4, 0.965, 0.811, 0)$ from Aghanim *et al.* (2020) for our subsequent analysis. We consider a radio interferometric array for the 21-cm observations mimicking the SKA1-mid. The SKA1-mid is one of the three different instruments that will be built as a part of the SKA telescope. SKA1-mid has 250 antennae. The diameter of each antenna is taken to be 13.5 m and system temperature (T_{sys}) assumed to be 40 K for the redshift $z = 2.3$. We also assume that the full frequency band will be subdivided into smaller frequency bands of 32 MHz. For Lyman-α forest observation, we have used the quasar number of distribution from DR14 of SDSS (Abolfathi *et al.* 2018). It has a total angular coverage of 14.555 deg^2 and we assumed the QSO number density, $\bar{n} = 60$ deg^{-2}. Each spectra is assumed to have been measured at $>3\sigma$ sensitivity.

We have divided the k-range from $0.1 < k < 1$ into 4 k-bins. We perform Fisher matrix analysis for the

Table 4. The 68% $(1 - \sigma)$ marginalized errors on $\log_{10}|f_{,R0}|$ and Ω_{m0} from the 21-cm and Lyman-α cross-correlation.

Model	$\log_{10}|f_{,R0}|$	Ω_{m0}
$f(R)$	-5 ± 0.29	0.315 ± 0.012

following parameters: the binned values of β_T, overall normalization factor ($\bar{\mathcal{N}}$), distortion factor ($\beta_{\mathcal{F}}$) and third order component of polynomial bias b_T. We have marginalized over all the parameters except the four values of β_T.

Figure 9 shows the $\beta_T(k, z)$ for $f(R)$ gravity models. The shaded region corresponds to the $1 - \sigma$ error projection for the fiducial $\log_{10}|f_{,R0}| = -5$ gravity model. At large scale, all $f(R)$ gravity theories match with standard ΛCDM model. However, we found that on small scales beyond ($k > 0.5$), the $\log_{10}|f_{,R0}| = -5$ model can be distinguished from ΛCDM model at a level of $3 - \sigma$ sensitivity, if we consider $2k$-bins for 500×60 h observation with 60 independent pointings. But, other $f(R)$ gravity models are not very much distinguishable ($<3 - \sigma$) throughout the k range. This is because at very higher redshifts, we expect all the modified gravity theories match to our standard concordance ΛCDM model and deviation from it, is much smaller. Instead of constraining the binned function $\beta_T(k)$, we investigate the possibility of putting bounds on $\log_{10}|f_{,R0}|$ from the given observation. Marginalizing over the overall amplitude of the power spectrum, we are thus interested in two parameters $(\Omega_{m0}, \log_{10}|f_{,R0}|)$. The error projections are given in Table 4.

6. Conclusion

Einstein's relativity has been extremely well tested on Solar system scales (Bertotti *et al.* 2003; Shapiro *et al.* 2004; Chiba *et al.* 2007). The $f(R)$ modification often confronts the strong agreement of general relativity on such small scales. Einstein's relativity can be recovered and Solar system tests can be evaded by the chameleon mechanism Khoury & Weltman (2004), Capozziello & Tsujikawa (2008) and Gu & Lin (2011). Effectively, this implies that $f(R)$ differs very little from R on solar system scales. It has been shown that Hu–Sawicki $f(R)$ gravity models agree well with the late-time cosmic acceleration without invoking a cosmological constant and satisfies both cosmological and Solar system tests in the weak-field limit (De Felice & Tsujikawa

2010). However, Solar system tests alone put only weak bounds on these models (Hu & Sawicki 2007a) and there is a great variability of model parameters. We have shown that the 21-cm intensity mapping instruments like SKA1 will be capable of constraining the a field value $\log_{10}|f_{,R0}| = -5 \pm 0.62$ of 68% confidence. This is an order of magnitude tighter than constraints currently available from galaxy cluster abundance (Ferraro *et al.* 2011). Further, Cataneo *et al.* (2015) showed that marginalized 95.4% upper limit on $\log_{10}|f_{,R0}| = -4.79$ using the cluster + Planck + WMAP + lensing + ACT + SPT + SN + BAO data. Joint analysis of 21-cm intensity mapping with the above observation probe shall be able to narrow down the current constraints. We note that the low redshift departure of $f(R)$ gravity from GR predictions is small and better modeling is needed to invoke non-linear chameleon suppression for tighter constraints on $f(R)$ models.

The radio-interferometric observation of the post-reionization HI 21-cm signal, thus holds the potential of providing robust constraints on $f(R)$ models. We have seen that the error projections from both the auto- and cross-correlation signals provide competitive bounds on $f(R)$ models. Several observational aspects, however, plague the detection of the 21-cm signal. We have evaded the key observational challenge arising from large astrophysical foregrounds that plague the signal. Astrophysical foregrounds from both galactic and extra galactic sources plague the signal and significant amount of foreground subtraction is required before one may detect the signal. Several methods of subtracting foregrounds have been suggested (see Ghosh *et al.* 2011 and citations in this work). Cross-correlation of the 21-cm signal has also been proposed as a way to mitigate the issue of large foregrounds (Guha Sarkar *et al.* 2010; Sarkar & Datta 2015). The cosmological origin of the 21-cm signal may only be ascertained in a cross-correlation. The foregrounds appear as noise in the cross-correlation and may be tackled by considering larger survey volumes. Further, man-made radio frequency interferences (RFIs), calibration errors and other observational systematics inhibits the sensitive detection of the HI 21-cm signal. A detailed study of these observational aspects shall be studied in a future work. We conclude by noting that future observation of the redshifted HI 21-cm signal shall be an important addition to the different cosmological probes aimed towards measuring possible modifications to Einstein's gravity. This shall enhance our understanding of late-time cosmological evolution and structure formation.

References

Abolfathi B., Aguado D., Aguilar G., *et al.* 2018, Astrophys. J. Suppl. Ser., 235, 42

Aghanim N., Akrami Y., Ashdown M., *et al.* 2020, Astron. Astrophys., 641, 6

Amendola L., Gannouji R., Polarski D., Tsujikawa S. 2007, Phys. Rev. D, 75, https://doi.org/10.1103/physrevd.75.083504

Amendola L., Tsujikawa S. 2010, Dark energy: Theory and observations (Cambridge University Press), https://doi.org/10.1017/CBO9780511750823

Armendariz-Picon C., Mukhanov V., Steinhardt P. J. 2001, Phys. Rev. D, 63, 103510

Arnold C., Fosalba P., Springel V., Puchwein E., Blot L. 2019, Mon. Not. R. Astron. Soc., 483, 790

Arnold C., Puchwein E., Springel V. 2015, Mon. Not. R. Astron. Soc., 448, 2275

Aviles A., Rodriguez-Meza M. A., De-Santiago J., Cervantes-Cota J. L. 2018, J. Cosmol. Astropart. Phys., 2018, 013

Baghram S., Rahvar S. 2010, J. Cosmol. Astropart. Phys., 2010, 008

Bagla J. S., Jassal H. K., Padmanabhan T. 2003, Phys. Rev. D, 67, 063504

Bagla J. S., Khandai N., Datta K. K. 2010, Mon. Not. R. Astron. Soc., 407, 567

Barboza E., Alcaniz J. 2008, Phys. Lett. B, 666, 415

Bento M. C., Bertolami O., Sen A. A. 2002, Phys. Rev. D, 66, 043507

Bertotti B., Iess L., Tortora, P. 2003, Nature, 425, 374

Bharadwaj S., Pandey S. K. 2003, J. Astrophys. Astron., 24, 23

Bharadwaj S., Ali S. S. 2004, Mon. Not. R. Astron. Soc., 352, 142

Bharadwaj S., Srikant P. S. 2004, J. Astrophys. Astron., 25, 67

Bharadwaj S., Sethi S. K. 2001, J. Astrophys. Astron., 22, 293

Bharadwaj S., Nath B. B., Sethi S. K. 2001, J. Astrophys. Astron., 22, 21

Bharadwaj S., Sethi S. K., Saini T. D. 2009, Phys. Rev. D, 79, 083538

Bharadwaj S., Sarkar A. K., Ali S. S. 2015, J. Astrophys. Astron., 36, 385

Boisseau B., Esposito-Farese G., Polarski D., Starobinsky A. A. 2000, Phys. Rev. Lett., 85, 2236

Brax P., Valageas P. 2019, J. Cosmol. Astropart. Phys., 2019, 049

Brax P., Van De Bruck C., Clesse S., Davis A.-C., Sculthorpe G. 2014, Phys. Rev. D, 89, 123507

Bull P., Ferreira P. G., Patel P., Santos M. G. 2015, Astrophys. J., 803, 21

Caldwell R. R., Dave R., Steinhardt P. J. 1998, Phys. Rev. Lett., 80, 1582

Capozziello S. 2002, Int. J. Mod. Phys. D, 11, 483

Capozziello S., Francaviglia M. 2008, Gen. Relativ. Gravit., 40, 357

Capozziello S., Tsujikawa S. 2008, Phys. Rev. D, 77, 107501

Carroll S. M. 2001, Living Rev. Relativ. 4, https://doi.org/10.12942/lrr-2001-1

Carroll S. M., Duvvuri V., Trodden M., Turner M. S. 2004, Phys. Rev. D, 70, 043528

Carucci I. P., Villaescusa-Navarro F., Viel M. 2017, J. Cosmol. Astropart. Phys., 2017, 001

Cataneo M., Rapetti D., Schmidt F., *et al.* 2015a, Phys. Rev. D, 92, 044009

Cataneo M., Rapetti D., Schmidt F., *et al.* 2015b, Phys. Rev. D, 92, https://doi.org/10.1103/physrevd.92.044009

Chang T., Pen U., Peterson J. B., McDonald P. 2008, Phys. Rev. Lett., 100, 091303

Chevallier M., David P. 2001, Int. J. Mod. Phys. D, 10, 213

Chiba T., Smith T. L., Erickcek A. L. 2007, Phys. Rev. D, 75, 124014

Cooke J., Wolfe A. M., Gawiser E., Prochaska J. X. 2006, Astrophys. J. Lett., 636, L9

Dash C. B., Guha Sarkar T. 2021, J. Cosmol. Astropart. Phys., 2021, 016

Dekel A., Lahav O. 1999, Astrophys. J., 520, 24

De Felice A., Tsujikawa S. 2010, Living Rev. Relat., 13, 1

Eisenstein D. J., Hu W. 1998, Astrophys. J., 496, 605

Fang L. Z., Bi H., Xiang S., Boerner G. 1993, Astrophys. J., 413, 477

Faraoni V. 2009, in 4th International Meeting on Gravitation and Cosmology (MGC 4), 19

Ferraro S., Schmidt F., Hu W. 2011, Phys. Rev. D, 83, 063503

Fry J. N. 1996, Astrophys. J. Letters, 461, L65

Gallerani S., Choudhury T. R., Ferrara A. 2006, Mon. Not. R. Astron. Soc., 370, 1401

Ghosh A., Bharadwaj S., Ali S. S., Chengalur J. N. 2011, Mon. Not. R. Astron. Soc., 418, 2584

Gu J.-A., Lin W.-T. 2011, arXiv preprint arXiv:1108.1782

Guha Sarkar T., Bharadwaj S., Choudhury T. R., Datta K. K. 2010, Mon. Not. R. Astron. Soc., 410, 1130

Guha Sarkar T., Mitra S., Majumdar S., Choudhury T. R. 2012, Mon. Not. R. Astron. Soc., 421, 3570

Heavens A. 2003, Mon. Not. R. Astron. Soc., 343, 1327

Higuchi Y., Shirasaki M. 2016, Mon. Not. R. Astron. Soc., 459, 2762

Hinshaw G., Spergel D. N., Verde L., *et al.* 2003, Astrophys. J. Suppl. Ser., 148, 135

Hoekstra H., Jain B. 2008, Annu. Rev. Nucl. Part. Sci., 58, 99

Hu W. 1999, Astrophys. J., 522, L21

Hu W., Sawicki I. 2007a, Phys. Rev. D, 76, https://doi.org/10.1103/physrevd.76.064004

Hu W., Sawicki I. 2007a, Phys. Rev. D, 76, https://doi.org/10.1103/physrevd.76.064004

Hu W., Sawicki I. 2007b, Phys. Rev. D, 76, 104043

Huterer D., Takada M., Bernstein G., Jain B. 2006, Mon. Not. R. Astron. Soc., 366, 101

Huterer D., White M. 2002, Astrophys. J., 578, L95

Jain B., Seljak U. 1997, Astrophys. J., 484, 560

Jana S., Mohanty S. 2019, Phys. Rev. D, 99, 044056

Khoury J., Weltman A. 2004, Phys. Rev. D, 69, https://doi.org/10.1103/physrevd.69.044026

Knox L., Albrecht A., Song Y. S. 2004, Weak Lensing and Supernovae: Complementary Probes of Dark Energy, arXiv:astro-ph/0408141

Lanzetta K. M., Wolfe A. M., Turnshek D. A. 1995a, Astrophys. J., 440, 435

Lanzetta K. M., Wolfe A. M., Turnshek D. A. 1995b, Astrophys. J., 440, 435

Li B., Hellwing W. A., Koyama K., *et al.* 2013, Mon. Not. R. Astron. Soc., 428, 743

Li B., Shirasaki M. 2018, Mon. Not. R. Astron. Soc., 474, 3599

Limber D. N. 1954, Astrophys. J., 119, 655

Linder E. V. 2003, Phys. Rev. Lett., 90, 091301

Liu X., Li B., Zhao G.-B., *et al.* 2016, Phys. Rev. Lett., 117, 051101

Loeb A., Wyithe J. S. B. 2008, Phys. Rev. Lett., 100, 161301

Loeb A., Zaldarriaga M. 2004, Phys. Rev. Lett., 92, 211301

Madau P., Meiksin A., Rees M. J. 1997, Astrophys. J., 475, 429

Madau P., Meiksin A., Rees M. J. 1997, Astrophys. J., 475, 429

Marchi F. D., Cascioli G. 2020, Class. Quantum Gravit., 37, 095007

Marín F. A., Gnedin N. Y., Seo H.-J., Vallinotto A. 2010, Astrophys. J., 718, 972

Miyazaki S., Hamana T., Ellis R. S., *et al.* 2007, Astrophys. J., 669, 714

Mo H. J., Jing Y. P., White S. D. M. 1996, Mon. Not. R. Astron. Soc., 282, 1096

Mo H. J., Mao S., White S. D. M. 1999, Mon. Not. R. Astron. Soc., 304, 175

Mota D. F., Shaw D. J. 2007, Phys. Rev. D, 75, 063501

Munshi D., Valageas P., Vanwaerbeke L., Heavens A. 2008, Phys. Rep., 462, 67

Nagamine K., Wolfe A. M., Hernquist L., Springel V. 2007, Astrophys. J., 660, 945

Nojiri S., Odintsov S. D. 2007, Int. J. Geom. Methods Mod. Phys., 4, 115

Nojiri S., Odintsov S. D., Sami M. 2006, Phys. Rev. D, 74, 046004

Noterdaeme P., Petitjean P., Ledoux C., Srianand R. 2009, Astron. Astrophys., 505, 1087

Obuljen A., Castorina E., Villaescusa-Navarro F., Viel M. 2018, J. Cosmol. Astropart. Phys., 2018, 004

Padmanabhan T. 2003, Phys. Rep., 380, 235

Padmanabhan T., Choudhury T. R. 2002, Phys. Rev. D, 66, 081301

Peirone S., Raveri M., Viel M., Borgani S., Ansoldi S. 2017, Phys. Rev.. D, 95, 023521

Perlmutter S., Gabi S., Goldhaber G., *et al.* 1997, Astrophys. J., 483, 565

Peroux C., McMahon R. G., Storrie-Lombardi L. J., Irwin M. J. 2003, Mon. Not. R. Astron. Soc., 346, 1103

Prochaska J. X., Herbert-Fort S., Wolfe A. M. 2005, Astrophys. J., 635, 123

Péroux C., McMahon R. G., Storrie-Lombardi L. J., Irwin M. J. 2003, Mon. Not. R. Astron. Soc., 346, 1103

Ratra B., Peebles P. J. E. 1988, Phys. Rev. D, 37, 3406

Riess A. G., Macri L. M., Hoffmann S. L., *et al.* 2016, Astrophys. J., 826, 56

Sarkar A. K., Bharadwaj S., Ali S. S. 2017a, J. Astrophys. Astron., 38, 14

Sarkar A. K., Bharadwaj S., Marthi V. R. 2017b, Mon. Not. R. Astron. Soc., 473, 261

Sarkar A. K., Bharadwaj S., Guha Sarkar T. 2018a, J. Cosmol. Astropart. Phys., 2018, 051

Sarkar A. K., Bharadwaj S., Sarkar T. G. 2018b, J. Cosmol. Astropart. Phys., 2018, 051

Sarkar T. G. 2010, J. Cosmol. Astropart. Phys., 2010, 002

Sarkar T. G., Datta K. K. 2015, J. Cosmol. Astropart. Phys., 2015, 001

Schmidt F., Vikhlinin A., Hu W. 2009, Phys. Rev. D, 80, 083505

Shapiro S. S., Davis J. L., Lebach D. E., Gregory J. 2004, Phys. Rev. Lett., 92, 121101

Song Y.-S., Hu W., Sawicki I. 2007, Phys. Rev. D, 75, 044004

Sotiriou T. P., Faraoni V. 2010, Rev. Mod. Phys., 82, 451

Sotiriou T. P., Liberati S. 2007, Ann. Phys., 322, 935

Spergel D. N., Verde L., Peiris H. V., *et al.* 2003, Astrophys. J. Suppl. Ser., 148, 175

Storrie-Lombardi L. J., McMahon R. G., Irwin M. J. 1996, Mon. Not. R. Astron. Soc., 283, L79

Subramanian K., Padmanabhan T. 1993, Mon. Not. R. Astron. Soc., 265, 101

Takada M., Jain B. 2003, Mon. Not. R. Astron. Soc., 344, 857

Takada M., Jain B. 2004, Mon. Not. R. Astron. Soc., 348, 897

Takada M., Jain B. 2009, Mon. Not. R. Astron. Soc., 395, 2065

Treu T. 2010, Annu. Rev. Astron. Astrophys., 48, 87

Tsujikawa S., Gannouji R., Moraes B., Polarski D. 2009, Phys. Rev. D, 80, 084044

Tsujikawa S., Uddin K., Mizuno S., Tavakol R., Yokoyama J. 2008, Phys. Rev. D, 77, 103009

Turner M. S., White M. 1997, Phys. Rev. D, 56, R4439

Visbal E., Loeb A., Wyithe S. 2009, J. Cosmol. Astro-Part. Phys., 10, 30

Waerbeke L. V., Mellier Y. 2003, Gravitational Lensing by Large Scale Structures: A Review, arXiv:astro-ph/030508

Weinberg S. 1989, Rev. Mod. Phys., 61, 1

Will C. M. 2014, Living Rev. Relat., 17, 1

Wolfe A. M., Gawiser E., Prochaska J. X. 2005, ARAA, 43, 861

Wyithe J. S. B., Loeb A. 2009, Mon. Not. R. Astron. Soc., 397, 1926

Wyithe S., Loeb A. 2007, ArXiv e-prints, arXiv:0708.3392

Wyithe S., Loeb A. 2008, ArXiv e-prints, arXiv:0808.2323

Yoshikawa K., Taruya A., Jing Y. P., Suto Y. 2001, Astrophys. J., 558, 520

Zafar T., Péroux C., Popping A., *et al.* 2013, Astron. Astrophys., 556, A141

Zhao G.-B., Raveri M., Pogosian L., *et al.* 2017, Nature Astron., 1, 627

Zwaan M. A., van der Hulst J. M., Briggs F. H., Verheijen M. A. W., Ryan-Weber E. V. 2005, Mon. Not. R. Astron. Soc., 364, 1467